Advances in Science and Technology Research Journal

Advances in Science and Technology Research Journal, 2026, 20(3), 479–493
https://doi.org/10.12913/22998624/214359
ISSN 2299-8624, License CC-BY 4.0

Received: 2025.10.23
Accepted: 2025.11.27
Published: 2026.02.01

Experimental determination of the pressure center shift in a wheelchair anti-rollback module based on contact force and rolling resistance torque

Bartosz Wieczorek[1*], Łukasz Warguła[1]

[1] Faculty of Mechanical Engineering, Poznan University of Technology, ul. Piotrowo 3, 60-965 Poznan, Poland
* Corresponding author's e-mail: bartosz.wieczorek@put.poznan.pl

ABSTRACT

The efficiency of manual wheelchair propulsion is largely determined by rolling resistance, which depends on tire pressure, surface type, and wheel construction. A particularly significant source of energy loss arises from anti-rollback modules, where the contact between a rigid roller and an elastic tire generates an additional braking torque. The aim of this study was to experimentally determine the displacement of the pressure center (x_0) within the contact zone between the roller of the anti-rollback module and the wheelchair tire, as a function of the normal load (F_0) and the internal tire pressure (p_t). The experiments were conducted using a custom-built test stand equipped with an HBM 1-T20WN torque transducer and a Zemic H3-C3 force sensor. The analysis included measurements of the braking torque (T_b) and the normal load across five pressure levels (3–8 bar) and eight loading conditions (25–200 N). The results showed that increasing tire pressure reduces tire deformation, enhances contact stiffness, and decreases the braking torque by approximately 10–15%. The displacement of the pressure center decreased with rising pressure: for F_0 = 25 N, x0 decreased from 11.6 mm (3 bar) to 9.1 mm (8 bar), and for F_0 = 200 N, from 18.5 mm to 16.0 mm. The linear model $x_0(F_0, p_t)$ achieved a determination coefficient of R^2 = 0.957, confirming its strong agreement with experimental data. The findings indicate that maintaining tire pressure within the range of 6–8 bar minimizes rolling resistance torque, thereby reducing user effort and improving propulsion efficiency.

Keywords: wheelchair, rolling resistance, tire pressure, braking torque, contact mechanics.

INTROCUTION

The efficiency of manual wheelchair propulsion is primarily determined by rolling resistance, which directly affects the user's effort and energy expenditure (1–3). The magnitude of rolling resistance depends on tire pressure, caster wheel diameter, surface type, and wheel configuration – higher pressure and larger casters reduce tire deformation, thereby minimizing energy losses and improving propulsion efficiency (4–6). Pneumatic tires generally exhibit lower rolling resistance compared to solid tires (4). Environmental factors, such as surface gradient and texture, also play a significant role (7,8). Moreover, additional components – such as anti-rollback modules – can increase the resistive torque (9). Ultimately, propulsion efficiency results from the combined interaction of mechanical, biomechanical, and environmental factors, which together determine the energetic cost and user comfort. In practical use, any additional resistive torque requires the wheelchair user to generate a higher propulsive moment with the upper limbs, leading to increased fatigue, reduced smoothness of motion, and a shorter range of mobility (4).

The sources of motion resistance in a wheelchair can be categorized into four main types: rolling resistance, bearing resistance, aerodynamic drag, and mechanical resistance arising from the operation of additional components, such as anti-rollback modules (1,10,11). Rolling resistance constitutes the primary component of forces

opposing motion and results from tire deformation during rolling on the surface. The magnitude of rolling resistance depends on tire pressure, surface type, tire design, and wheel load (4,12,13). Additional mechanical resistance is generated by anti-rollback modules, in which the contact between the roller and the tire produces a braking torque that can increase the total rolling resistance by as much as 30–75% (14). In this study, the braking torque (Tb) refers exclusively to the resistive moment generated by the roller–tire contact in the anti-rollback module. It represents a specific mechanical component of the total rolling resistance torque acting on the wheelchair wheel. This specific contact – between the elastic tire and the rigid roller – determines the generated braking torque, which, on one hand, provides a safety function by preventing backward motion through the creation of a frictional moment, and on the other hand, may negatively affect ride comfort by increasing the resistive torque during uphill propulsion.

This phenomenon should be analyzed in the context of pneumatic tire contact mechanics, as described by Hertzian theory, according to which the contact between an elastic surface and a rigid body results in the formation of an elliptical contact area the dimensions and pressure distribution of which depend on geometry, normal load, and material stiffness (15,16). In the case of a pneumatic tire, the Hertz model allows estimation of the shape and size of the contact area; however, its accuracy decreases under dynamic conditions, when the pressure distribution changes due to varying loads and frictional effects (17–19).

In the case of a pneumatic tire, the key factor determining the pressure distribution is the internal pressure, which influences both the effective contact radius and the radial deflection of the tire (20–22). Lower pressure results in greater deflection and elongation of the contact patch, while higher pressure shortens it and increases local contact stresses (23). As the pressure rises, the contact area becomes shorter and more concentrated, leading to a shift of the pressure center relative to the vertical axis of the wheel (23,24). This shift in the pressure center is directly related to the rolling resistance torque, which, in the roller–tire system manifests as a braking torque (T_b) opposing the rotational motion..

The literature indicates that both the contact length and tire deflection increase linearly with load, leading to higher rolling resistance (25,26). These relationships have been confirmed for automotive and industrial tires (27,28); however, there is a lack of experimental research concerning small-scale systems such as anti-rollback modules in manual wheelchairs. The specificity of these modules lies in the fact that the roller interacting with the tire has a small radius and rotates freely, which, combined with a limited contact area, results in an atypical stress distribution and a displacement of the pressure center in the direction of rolling motion. This phenomenon directly affects the magnitude of the braking torque, and its quantitative characterization represents an important step toward the modeling and optimization of such mechanisms.

The objective of this study was to estimate the position of the pressure center x_0 **na podstawie momentu oporów toczenia T_b powstającego w wyniku kontaktu rolki modułu blokady cofania z oponą koła wózka inwalidzkiego. Realizacja tego celu wymaga wyznaczenia zależności między momentem oporów T_b a siłą docisku rolki F. Osiągnięcie celu badawczego umożliwi również weryfikację hipotezy, zgodnie z którą współczynnik proporcjonalności przesunięcia środka nacisków η pozostaje niezależny od siły docisku w zakresie typowym dla eksploatacyjnych obciążeń opony wózka inwalidzkiego.**

METHODS AND MATERIALS

Materials

To investigate the braking torque (T_b) under the influence of the normal load (F), a custom-designed experimental test stand was developed (Figure 1). The measurement of the braking torque T_b was based on the methodology commonly used for torque and power measurements in engine dynamometers (29,30). The main component of the test stand was a high-precision torque transducer manufactured by HBM (Darmstadt, Germany), model 1-T20WN/100Nm, featuring an accuracy class of 0.2, a measurement range of 100 Nm, a resolution of 0.001 Nm, and a sampling frequency of 100 Hz. The torque transducer connected the shaft, on which the wheelchair wheel was mounted, with the drive system. The drive was provided by a three-phase electric motor manufactured by BESEL S.A. (Brzeg, Poland), rated at 2.2 kW, with a rotational speed of 2820 rpm and an efficiency of 80%. The motor

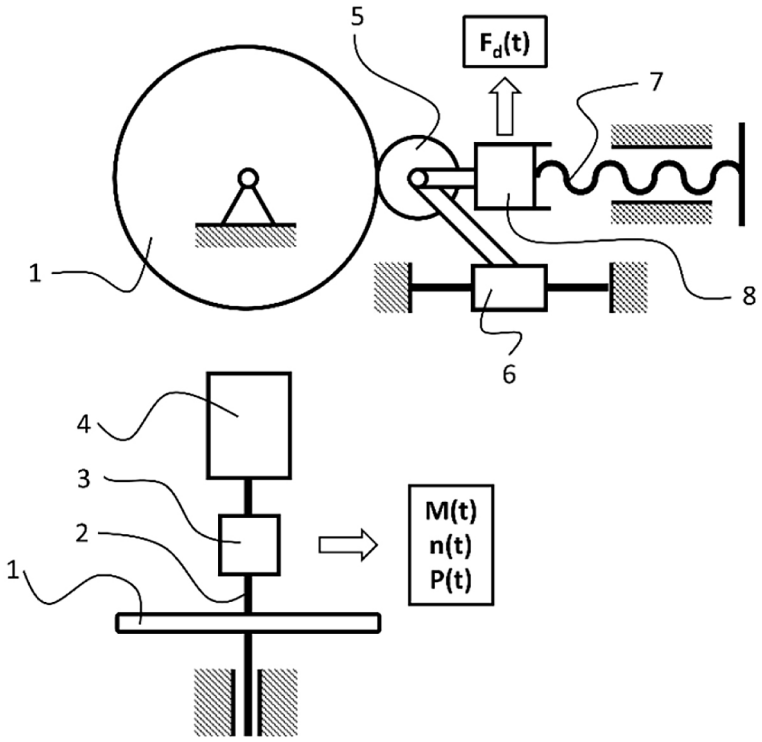

Figure 1. Schematic diagram of the experimental test stand used in the study. Where: 1 – wheelchair wheel, 2 – shaft, 3 – torque transducer, 4 – electric motor, 5 – tested roller of the anti-rollback module, 6 – linear guide system, 7 – loading screw, 8 – normal force sensor

was coupled with a planetary gearbox, model UDL 020 (ROKMAN DRIVE), featuring an adjustable transmission ratio ranging from 1.4:1 to 7:1. The motor–gearbox assembly served solely to induce rotational motion of the wheel. The driving torque (Td) and rotational speed (n) were recorded by the torque transducer, allowing subsequent analysis of motion resistance as a function of the applied normal load. The tested roller of the anti-rollback module was pressed against the tire using a screw-driven loading mechanism guided by linear bearings. The normal load (F) was measured with a strain-gauge force sensor manufactured by Zemic (Hengelo, Netherlands), model H3-C3-100 kg, with a measurement range of 1000 N and an absolute measurement error of 0.02%. This sensor served as a coupling element between the loading mechanism and the tested roller, enabling both the adjustment of the preset load and its continuous monitoring during the experiment. Such a configuration allowed precise and repeatable measurement of the resistive torque generated by the contact between the roller and the rotating wheel under controlled normal loading conditions, providing the basis for further analysis of the effects of normal force and internal tire pressure on the braking torque magnitude.

In the study, a prototype composite roller of the anti-rollback module (Patent Application No. P.450537, Polish Patent Office) (Figure 2) was used as a non-deformable roller. The roller, with a radius (RR) of 30 mm, consisted of four functional layers. The inner core was made of PLA material using 3D printing technology with 80% infill, providing adequate structural stiffness. On top of this core, an elastic layer made of TPU (thermoplastic polyurethane) with a hardness of 55° Shore and 100% infill was printed, serving as a damping element and improving component durability. The outer rigid structure consisted of a second PLA (polylactide) ring with 80% infill, to which a tread layer made of NBR (nitrile butadiene rubber) was permanently vulcanized. The wheelchair drive wheel, against which the roller was pressed, consisted of a 24-inch rim fitted with a Gazelle 24x1” tire manufactured by MBL (Brøndby, Denmark). This tire was selected due to its widespread use in adult manual wheelchairs. The Gazelle model features a two-layer construction made of woven SPL-type nylon with a high thread density of 127 TPI, ensuring appropriate flexibility and durability under typical operating conditions. The reinforcement insert has a width of 15 mm,

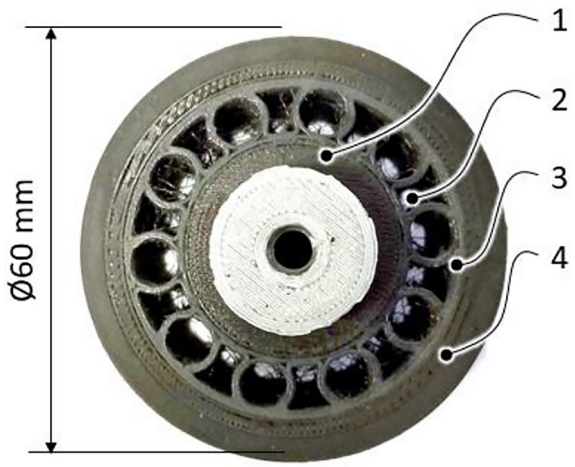

Figure 2. Composite roller of the anti-rollback module used in the study, where:
1 – rigid PLA core (polylactide),
2 – elastic TPU core (thermoplastic polyurethane),
3 – rigid PLA ring (polylactide),
4 – NBR tread (nitrile butadiene rubber)

and the recommended inflation pressure range is between 6 and 10 bar. The choice of this tire enabled the experiments to be conducted using a standard and widely adopted configuration of a wheelchair drive wheel (4).

Measurement procedure

The measurements were carried out for five tire pressure values pt (3, 4, 5, 6, and 7 bar) and initial normal loads F ranging from 25 N to 200 N, with an interval of 25 N. Before each test, the roller of the anti-rollback module was positioned at the same point on the circumference of the wheelchair wheel to ensure repeatability of contact conditions and the initial normal load setting F. Then, using the loading screw mechanism (7) (Figure 1), the initial normal load F was adjusted to the target value. Prior to each measurement, both the torque transducer and the force sensor were zeroed. After the system was activated, the time histories of the normal load F(t) and the driving torque $T_b(t)$ were recorded. On the basis of the time variation of the force signal, one complete wheel revolution was identified, and the rotation time t_0 was determined. For each dataset, the segments corresponding to one full revolution were extracted, and the average normal load (avg. F) and the corresponding average resistive torque (avg. T_b) were calculated. An example of this process, based on the function F(t), is shown in Figure 3.

According to the adopted procedure, in the first step (A), the wheel was positioned at the initial starting point, and the initial normal load F was set. Next, the measurement was performed, and based on the analysis of signal extrema, the recorded data were divided into time intervals t0 corresponding to one full wheel revolution (B). The extracted intervals were then normalized with respect to one complete rotation, expressing the independent variable as a dimensionless phase quantity φ ranging from 0 to 100% (C). A φ value of 100% represented one full revolution of the wheelchair wheel. For each normalized force waveform F(φ), the mean variation of the normal load Fmed(φ) corresponding to one wheel revolution was calculated (D). On the basis of the Fmed function, the average normal load avg. F was determined, taking into account its fluctuation relative to the initial value caused by wheel noncircularity (E). The applied signal processing algorithm followed the phase normalization and cycle-averaging procedure (31,32) commonly used in the analysis of periodic phenomena in mechanical engineering and biomechanics. Such methods are typically employed in studies of tire rolling resistance torque (33), analyses of wheelchair propulsion cycles (34) and diagnostics of rotating systems using order analysis (35).

Analytical model

The main assumption in the adopted method for determining the pressure center (x_0) is that the contact dimension between the tire and the non-deformable surface remains constant, regardless of the driving torque applied to the wheel (36–38). Only the displacement of the pressure center caused by the rolling motion of the tire, denoted as x_0, changes (39). Additionally, a symmetric pressure distribution was assumed in the direction transverse to the wheel's plane of rotation. The final assumption was that, relative to the wheelchair tire, the pressed roller is non-deformable.

To describe the motion conditions of the wheelchair wheel in contact with the roller of the anti-rollback module, a simplified analytical model based on torque equilibrium was adopted. For the wheel to rotate, the driving torque (T_d) must exceed the braking torque (T_b) generated by the roller's normal load acting on the tire. Additionally, other resistive torques (T_R) must be considered, including those resulting from bearing friction, rolling resistance, and tire deformation losses.

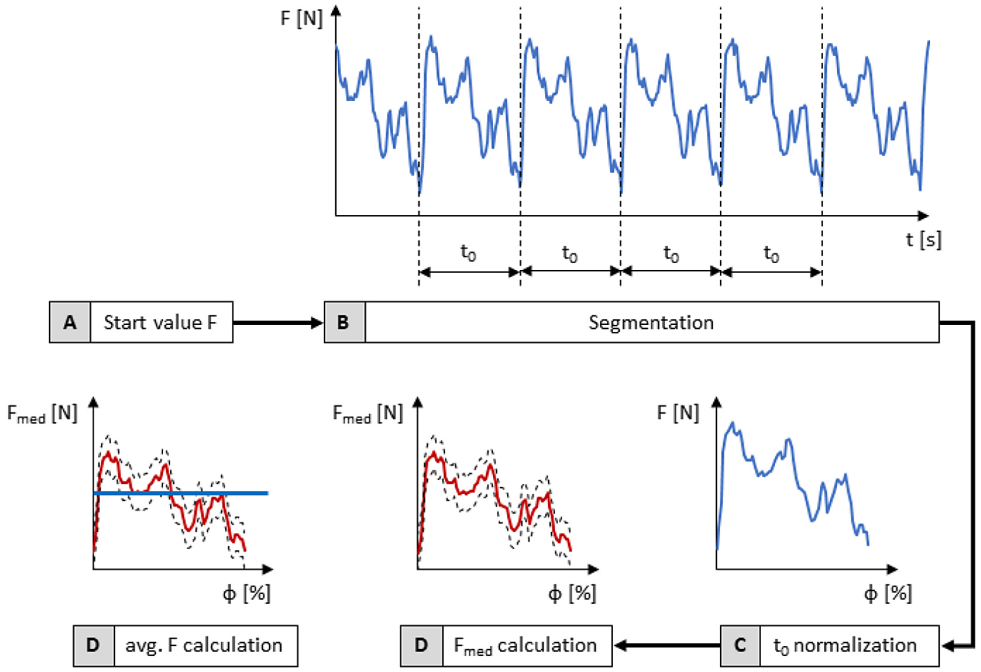

Figure 3. Signal processing algorithm, where F – normal load, t_0 – duration of one full revolution of the wheelchair wheel, φ – dimensionless time value corresponding to one wheel revolution, Fmed – mean value of the normal load function for one wheel revolution, avg. F – average normal load resulting from the initial setting and the curvature of the wheelchair wheel

The condition enabling the initiation of motion can therefore be expressed as the inequality (1):

$$T_d > T_b + T_R \tag{1}$$

where: T_d – driving torque, T_b – braking torque generated by the roller's normal load, T_R – resistive torque resulting from all other motion resistance forces not included in the present analysis.

The presented system represents a simplified analytical model in which secondary factors such as slip, tire material hysteresis, and local variations in tire stiffness are neglected (40–42). In the present study, the analysis was intentionally limited to quasi-static conditions. The wheel was rotated at a constant low speed (n = 60 rpm), without acceleration or inclination of the test stand, ensuring that inertial and dynamic effects were negligible. Hysteresis losses were assumed constant within each measurement cycle, and their influence was included in the averaged torque signal. Consequently, the presented model represents static equilibrium states that accurately describe low-speed interactions between the roller and the tire, allowing the findings to be generalized to typical manual wheelchair propulsion conditions. These factors are either absent or have a marginal effect on the overall characteristics of the phenomenon, and their omission does not introduce significant deviations in assessing the relationship between the braking torque (T_b) and the distribution of contact pressures. In the presented analytical problem, the unknown quantity is the distance x_0. Using the measured braking torque (T_b) and the known normal load applied by the roller (F), the value of x_0 can be calculated according to Equation 2.

$$x_0 = \frac{T_b}{F} \tag{2}$$

Equation 2 forms the basis for further analysis, enabling the determination of the pressure center displacement based on experimentally measured values of braking torque (T_b) and normal load (F). In practice, it allows for the indirect estimation of the position of the contact reaction center, the variation of which is crucial for describing the rolling resistance torque and analyzing the effectiveness of operation of the anti-rollback module.

RESULTS

During the experiments, the independent variable was the nominal normal load F_0, adjusted manually by the operator. However, this value

varied with the rotation of the tested wheelchair wheel due to its geometric noncircularity (43). Therefore, as a first step, the average normal load values were determined for the tested range of nominal loads F_0. The mean normal load (avg. F) was calculated in accordance with the previously described experimental methodology, and this analysis was performed for the entire test range (Figure 4, Table 1). On the basis of the obtained results, it was found that the actual mean normal load F_{avg} was significantly higher than the nominal load F_0 set during the tests. Across the entire range of analyzed pressures (3–8 bar), the values of F_{avg} ranged from approximately 37.9 N for F_0 = 25 N to 237.9 N for F_0 = 200 N. This indicates that, under static conditions, the actual normal load was on average 17.8 ± 2.3% higher than the nominal value set by the operator. The largest discrepancies were observed at lower F_0 values, where the relative excess of F_{avg} exceeded 40%, while with increasing F_0, this difference decreased to around 10%. Furthermore, a clear influence of tire pressure on the average normal load value was demonstrated. As the tire pressure increased from 3 to 8 bar, F_{avg} systematically increased for all nominal load levels F_0, showing an average rise of approximately 13–15%. The greatest increase in reaction force was observed at lower F_0 values, indicating that the stiffening effect of the tire resulting from higher internal pressure is nonlinear in nature (44,45) and particularly pronounced in the low-load range (46).

To assess the effect of tire pressure on the mean normal load (avg. F), a one-way analysis of variance (ANOVA) was conducted, in which the independent factor was tire pressure in the range of 3–8 bar, and the dependent variable was the mean reaction force F_{avg} (Table 2). The analysis, performed for n = 48 observations (8 load levels F0 × 6 pressure levels), revealed a statistically significant effect of pressure on F_{avg} ($F(5,42) = 6.21$; $p = 0.0004$). The effect size, expressed by $\eta^2 = 0.43$, indicated a large influence of the factor, while the high test power ($1-\beta = 0.91$) confirmed the reliability of the obtained result. Verification of test assumptions confirmed that the criteria of normality (Shapiro–Wilk test, $p > 0.05$) and homogeneity of variances (Levene's test, $p > 0.05$) were satisfied. The Tukey post-hoc test showed that significant differences occurred primarily between the extreme pressure values (3 and 8 bar, $p < 0.01$). The obtained results clearly demonstrate that increasing tire pressure leads to an increase in the average normal load, resulting from the reduction of tire deformation and the corresponding increase in contact stiffness. Although the experimental design enabled a two-factor analysis ($F_0 \times p_t$), the one-way ANOVA was selected intentionally to isolate the influence of tire pressure on the dependent variables. The normal load F_0 was treated as a continuous, experimentally controlled parameter analyzed separately through regression relationships and graphical dependencies. This approach ensured statistical consistency with the subsequent regression model describing the displacement of the pressure center $x_0(F_0, p_t)$ and avoided artificial categorization of continuous variables.

Simultaneously with the measurement of the variation in normal load relative to the nominal

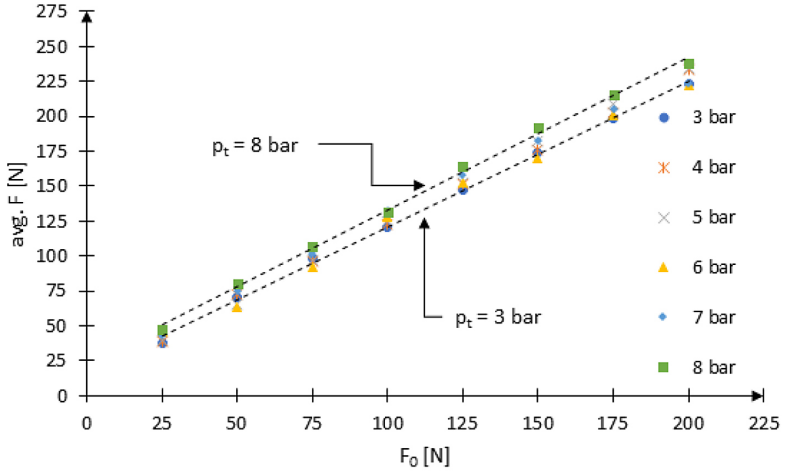

Figure 4. Graph of the variation of the average normal load (avg. F) as a function of the nominal normal load (F_0) for the tested ranges of the wheelchair tire internal pressure (p_t)

Table 1. Results of the average normal load (avg. F) as a function of the initial normal load (F_0) and the curvature of the wheelchair wheel, where p – assumed level of significance

F_0 [N]	Parameter	3 bar	4 bar	5 bar	6 bar	7 bar	8 bar
25	avg. F [N]	37.9	39.2	39.3	45.8	43.5	47.1
	p=0.05	2.6	2.1	2.5	2.8	2.6	2.9
50	avg. F [N]	71.0	72.2	64.9	62.9	75.5	80.1
	p=0.05	2.4	2.1	2.3	2.5	3.0	3.2
75	avg. F [N]	97.7	96.0	97.4	92.2	102.0	107.1
	p=0.05	2.3	2.2	2.8	2.7	3.0	3.1
100	avg. F [N]	120.6	122.3	124.3	127.6	132.3	131.8
	p=0.05	1.8	1.8	2.4	2.7	3.1	4.2
125	avg. F [N]	147.1	151.7	152.5	152.5	157.7	164.0
	p=0.05	1.7	2.0	2.1	2.4	3.1	3.4
150	avg. F [N]	173.6	176.3	182.2	170.0	182.8	191.7
	p=0.05	1.3	2.1	2.0	2.2	3.0	3.4
175	avg. F [N]	198.5	202.8	209.2	200.2	205.6	215.0
	p=0.05	1.4	1.8	2.2	2.6	2.9	3.2
200	avg. F [N]	223.6	233.7	233.9	222.2	223.6	237.9
	p=0.05	1.4	1.4	2.9	2.2	3.2	3.3

Table 2. Results of the statistical analysis of the effect of tire pressure on the mean normal load (avg. F)

Statistical indicator	Symbol	Value	Interpretation
Sample size	n	48	8 × 6 measurements
Degrees of freedom	$df_{1,2}$	5, 42	Factor/error
ANOVA test value	F	6.21	Significant factor effect
Statistical significance	p	0.0004	($p < 0.001$)
Effect size	η^2	0.43	Large
Test power	1-β	0.91	High
Normality test	—	($p > 0.05$)	Assumption met
Variance homogeneity test	—	($p > 0.05$)	Assumption met
Tukey HSD post-hoc test	—	($p < 0.01$)	Differences: 3–8 bar

force F_0, the braking torque introduced into the drive system by the roller of the anti-rollback module was also measured. These results are presented as a function of the independent variable F_0 (Figure 5, Table 3). The obtained data showed that as the normal load F_0 increased, the braking torque T_b rose almost linearly, while increasing tire pressure caused a systematic decrease in the average braking torque avg. T_b. For the lowest load (F_0 = 25 N), the braking torque ranged from 0.41 Nm (at 4 bar) to 0.46 Nm (at 7 bar), whereas for the highest load (F_0 = 200 N), it ranged from 3.81 Nm (at 8 bar) to 4.14 Nm (at 3 bar). The relationship $T_b(F_0)$ exhibited a quasi-linear character within the tested range of loads and pressures.

The analysis showed that increasing tire pressure led to a reduction in the braking torque across the entire range of loads. For example, at F_0 = 100 N, the average braking torque (avg. Tb) decreased from 2.04 Nm (at 3 bar) to 1.61 Nm (at 8 bar), representing a reduction of approximately 21%. For the highest load (F_0 = 200 N), the difference between the extreme values was 0.33 Nm, or about 8%. This indicates that the influence of pressure was most pronounced at lower normal loads, while the effect diminished with increasing F_0. The slope of the avg. $T_b(F_0)$ characteristics decreased as tire pressure increased, confirming that the rate of braking torque growth as a function of F_0 was smaller at higher pressures. For a pressure of 3 bar, the trend line slope was approximately 0.019 Nm/N, while at 8 bar it decreased to about 0.017 Nm/N. However, the linear nature of the avg. $T_b(F_0)$ relationship should be considered valid only within the tested

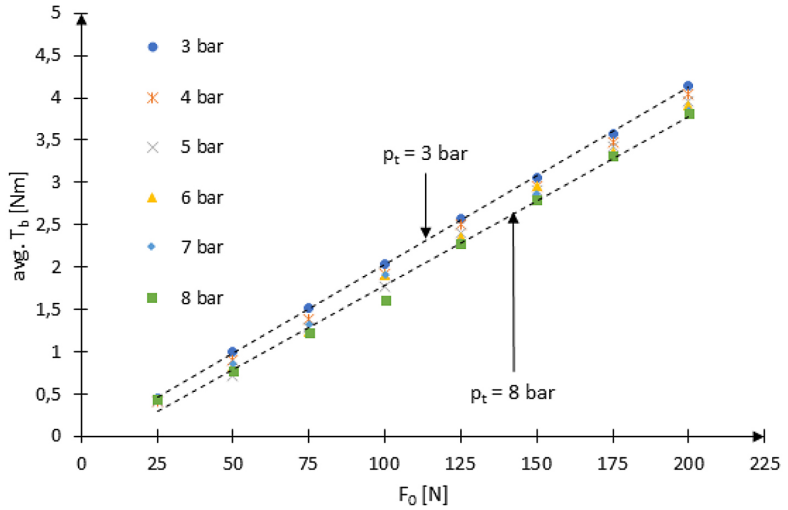

Figure 5. Graph of the variation of the average braking torque caused by the roller load (avg. T_b) as a function of the nominal normal load (F_0) for the tested ranges of the wheelchair tire's internal pressure (p_t)

Table 3. Results of the average braking torque caused by the roller load (avg. T_b) as a function of the initial normal load (F_0) and the curvature of the wheelchair wheel, where p – assumed level of significance

F_0 [N]	Parameter	3 bar	4 bar	5 bar	6 bar	7 bar	8 bar
25	avg. T_b [Nm]	0.44	0.41	0.42	0.43	0.46	0.43
	p=0.05	0.04	0.04	0.03	0.04	0.03	0.03
50	avg. T_b [Nm]	1.00	0.89	0.72	0.82	0.85	0.78
	p=0.05	0.05	0.06	0.05	0.05	0.05	0.05
75	avg. T_b [Nm]	1.52	1.39	1.28	1.24	1.32	1.22
	p=0.05	0.04	0.06	0.05	0.05	0.06	0.05
100	avg. T_b [Nm]	2.04	1.92	1.76	1.90	1.91	1.61
	p=0.05	0.04	0.05	0.05	0.05	0.05	0.06
125	avg. T_b [Nm]	2.57	2.50	2.40	2.35	2.30	2.28
	p=0.05	0.04	0.05	0.04	0.04	0.05	0.05
150	avg. T_b [Nm]	3.05	2.95	2.90	2.96	2.86	2.80
	p=0.05	0.03	0.05	0.04	0.03	0.05	0.05
175	avg. T_b [Nm]	3.57	3.47	3.42	3.35	3.30	3.31
	p=0.05	0.03	0.03	0.04	0.03	0.04	0.05
200	avg. T_b [Nm]	4.14	4.04	3.95	3.90	3.85	3.81
	p=0.05	0.03	0.03	0.03	0.03	0.03	0.04

range (F_0 = 25–200 N, p_t = 3–8 bar). At higher normal loads, a transition to a nonlinear trend can be expected, resulting from localized deformation saturation and changes in the contact stiffness between the roller and the tire. The upper limit of F_0 = 200 N was set due to structural constraints. At higher loads, permanent deformations and damage were observed in the composite roller used in the anti-rollback module, which prevented further increases in the applied normal load.

To evaluate the relationship between tire internal pressure and the average braking torque (avg. Tb), a one-way analysis of variance (ANOVA) was performed (Table 4). In this analysis, the independent factor was tire pressure in the range of 3–8 bar, while the dependent variable was the mean value of the braking torque obtained for each initial normal load Fo. In total, n = 48 observations were analyzed (8 load levels F_0 × 6 pressure levels). The results of the test revealed a statistically significant effect of pressure on the braking torque ($F(5,42) = 9.34$; $p = 0.00002$), indicating that changes in pressure significantly modify the response characteristics of the roller–tire

system. The estimated effect size coefficient $\eta^2 = 0.53$ confirmed a very strong influence of the tested factor, and the high test power ($1-\beta = 0.96$) demonstrated the high reliability of the obtained results. Verification of the test assumptions confirmed compliance with the criteria of normality (Shapiro–Wilk test, $p > 0.05$) and homogeneity of variances (Levene's test, $p > 0.05$). The post-hoc analysis (Tukey HSD test) showed that significant differences occurred mainly between the avg. T_b values for the extreme pressure levels (3 and 8 bar, $p < 0.001$), and to a lesser extent between intermediate levels (4–7 bar, $p < 0.05$).

In the next stage of the study, the displacement of the pressure center (x_0) was determined, calculated as the ratio of the average braking torque (avg. T_b) to the average normal load (avg. F). The independent variable was the nominal normal load F0, ranging from 25 to 200 N, while the conditioning factor was the tire pressure pt, taking values from 3 to 8 bar (Table 5). The displacement of the pressure center increased with rising normal load F0, regardless of the tire pressure value. For the lowest load (F_0 = 25 N), x_0 ranged from approximately 9.1 mm (at 8 bar) to 11.6 mm (at 3 bar), whereas for the highest load (F_0 = 200 N), it ranged from 16.0 mm (at 8 bar) to 18.5 mm (at 3 bar). This indicates that, within the analyzed range of normal loads, the average displacement of the pressure center increased by approximately 60%, with the rate of change being more pronounced at lower F_0 values.

A comparison of the values obtained for different tire pressure levels (p_t) showed that increasing pressure resulted in a systematic decrease in x_0. For each value of F_0, the highest displacement occurred at 3 bar and the lowest at 8 bar. The average reduction in x_0 between these extreme pressure levels ranged from approximately 20% for low normal loads (25–50 N) to about 15% for higher loads (150–200 N).

The analysis of the obtained characteristics showed that the relationship $x_0(F_0)$ is generally close to linear, although at lower pressures (3–4 bar) a slight curvilinear deviation is visible, resulting from the greater deformability of the tire. For higher pressures (6–8 bar), this relationship is almost perfectly linear, and the trend lines can be considered parallel, indicating a similar influence of the normal load F_0 on the displacement of the pressure center x_0. According to the tire manufacturer's recommendations, the operational pressure range is 6–10 bar (47,48). However, in practical wheelchair use, pressures up to 8 bar are typically applied (49), corresponding to the capacity of standard home compressors. Therefore, for further analysis, it was assumed that within the examined range of F_0 = 25–200 N and p_t = 3–8 bar, the relationship $x_0(F_0, p_t)$ can be represented by a simplified linear model described by Equation 3.

$$x_0(F_0, p_t) \approx a \cdot F_0 + b_0 - c \cdot p_t \qquad (3)$$

where: a – slope coefficient of the function, constant for the entire range of tested tire pressures (p_t); F_0 – initial normal load of the roller applied to the wheel; b_0 – intercept term representing the initial displacement level resulting from the internal resistance of the bearing system; c – coefficient describing the decrease in the pressure center displacement as a function of tire pressure (p_t).

On the basis of the conducted experiments and the obtained numerical data, the values of the above coefficients were determined (4). It should be noted that these values are valid only

Table 4. Results of the statistical analysis of the effect of tire pressure on the average braking torque (avg. T_b)

Statistical indicator	Symbol	Value	Interpretation
Sample size	n	48	8 × 6 measurements
Degrees of freedom	$df_{1,2}$	5, 42	Factor/error
ANOVA test value	F	9.34	Significant factor effect
Statistical significance	p	0.00002	($p < 0.001$)
Effect size	η^2	0.53	Very large
Test power	$1-\beta$	0.96	High
Normality test	—	($p > 0.05$)	Assumption met
Variance homogeneity test	—	($p > 0.05$)	Assumption met
Tukey HSD post-hoc test	—	($p < 0.001$)	Differences: 3–8 bar, partially 4–7 bar

within the tested ranges of normal load (F_0) and tire pressure (p_t) (Figure 6). Moreover, they incorporate material constants related to the tested tire, its structural design, and the curvature of the drive wheel rim. However, in this study, one of the most commonly used wheelchair tire models was adopted, and the rim curvature corresponded to standard factory centering conditions for a new wheelchair wheel.

$$x_0 \approx 0.0387 \cdot F_0 + 13.24 - \\ -0.558 \cdot p_t \quad (4)$$

The regression model fitting was performed using the least squares method based on 48 measurement points. The dataset included eight levels of normal load and six levels of tire pressure. The linear model accurately reflected the measurement results, with a coefficient of determination $R^2 = 0.957$, indicating that more than 95% of the variability in x_0 values was explained by the normal load F_0 and tire pressure p_t. The model's significance was confirmed by the F-test, which yielded $F(2,45) = 499.3$ at $p < 0.0001$. All regression coefficients were statistically significant ($p < 0.001$), indicating that both F_0 and p_t have a significant influence on x_0. Verification of the regression assumptions confirmed the normality of residuals (Shapiro–Wilk test, $p > 0.05$) and the homogeneity of variances (Breusch–Pagan test, $p > 0.05$). Additionally, low Variance Inflation Factor (VIF < 2) values confirmed the absence of multicollinearity between the variables. The obtained results demonstrate that the model is well-fitted and statistically valid, and therefore it can be reliably used to analyze the displacement of the pressure center in the roller–tire contact zone.

DISCUSSION

The conducted research confirmed that tire pressure has a pronounced influence on the behavior and characteristics of forces and torques in the contact zone between the roller and the tire of a wheelchair drive wheel. As the pressure increased from 3 to 8 bar, the actual average normal load (avg. F) rose by approximately 10–40% relative to the nominal value (F_0), depending on the load level. Higher pressure increased tire stiffness and reduced deformation, resulting in more stable contact with the roller and a more uniform pressure distribution within the contact area. Similar relationships have been reported in the studies on rolling resistance in wheelchairs, which demonstrated that lower tire pressure increases the force required to initiate wheel motion and the user's effort during propulsion (50,51). Maintaining the recommended tire pressure reduces rolling resistance forces and decreases the load on upper limb muscles, thereby lowering the energy expenditure during wheelchair propulsion (48). An increase in

Table 5. Results of the pressure center displacement (x0) as a function of the initial normal load (F0) and tire pressure (pt), where p – assumed level of significance

F_0 [N]	Parameter	3 bar	4 bar	5 bar	6 bar	7 bar	8 bar
25	x_0 [mm]	11.61	10.46	10.69	9.39	10.57	9.13
	p=0.05	1.32	1.16	1.02	1.05	0.94	0.85
50	x_0 [mm]	14.08	12.33	11.09	13.04	11.26	9.74
	p=0.05	0.85	0.91	0.86	0.95	0.80	0.74
75	x_0 [mm]	15.56	14.48	13.14	13.45	12.94	11.39
	p=0.05	0.55	0.71	0.64	0.67	0.70	0.57
100	x_0 [mm]	16.92	15.70	14.16	14.89	14.44	12.22
	p=0.05	0.42	0.47	0.49	0.50	0.51	0.60
125	x_0 [mm]	17.47	16.48	15.74	15.41	14.58	13.90
	p=0.05	0.34	0.39	0.34	0.36	0.43	0.42
150	x_0 [mm]	17.57	16.73	15.92	17.41	15.65	14.61
	p=0.05	0.22	0.35	0.28	0.29	0.38	0.37
175	x_0 [mm]	17.98	17.11	16.35	16.73	16.05	15.40
	p=0.05	0.20	0.21	0.26	0.26	0.30	0.33
200	x_0 [mm]	18.52	17.29	16.89	17.55	17.22	16.02
	p=0.05	0.18	0.16	0.25	0.22	0.28	0.28

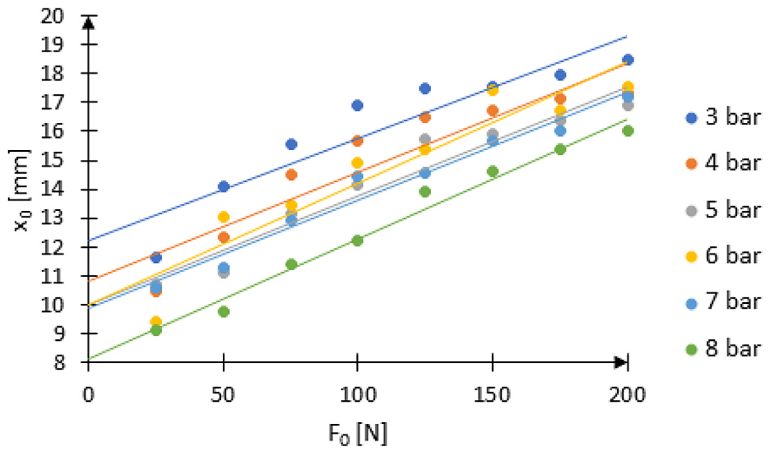

Figure 6. Graph of the variation of the pressure center displacement (x_0) as a function of the nominal normal load (F_0) for the tested ranges of the wheelchair tire's internal pressure (p_t)

tire pressure reduced deformation and increased contact stiffness. As a result, the reaction force became more stable, and the avg. $F(F_0)$ relationship exhibited a more linear trend. Raising the pressure from 3 to 8 bar led to a reduction in braking torque (Tb) by approximately 10–15% across the entire range of normal loads. This behavior is consistent with the mechanical properties of tires described in the literature, where higher pressure enhances contact stiffness and stabilizes the forces within the contact zone (24,52). Pressure variation also affects the shape of the contact patch, which changes from trapezoidal to more rectangular, while the contact pressure increases, improving stability and predictability of tire behavior (52). Studies have also shown that higher tire pressures increase both vertical and lateral stiffness, stabilizing braking forces and facilitating control of the system under load (53). At the same time, higher pressure may slightly reduce ride comfort, as more vibrations are transmitted to the wheelchair structure and the user (54).

The braking torque (T_b) values increased proportionally to the normal load (F_0), confirming a linear characteristic within the tested range. For low load values (F_0 = 25 N), the braking torque rose from 0.43 Nm at 8 bar to 0.44 Nm at 3 bar, while for the highest load (F_0 = 200 N), it increased from 3.81 Nm to 4.14 Nm. Increasing the tire pressure led to a reduction in the contact area between the roller and the tire, which caused a shift of the pressure center and, consequently, a decrease in the braking torque T_b. The highest torque values occurred at lower pressures (3–4 bar), resulting from greater tire deformation and a rearward shift of the pressure center within the contact zone. This phenomenon aligns with previous findings, which indicate that lower tire pressure increases deformation and leads to higher braking torque (51,55). Greater tire deflection shifts the region of maximum pressure opposite to the roller's rolling direction, increasing the lever arm of the resistive force and thus the braking torque.

The relationship between the pressure center displacement (x_0) and the normal load (F_0) showed a systematic decrease in x_0 with increasing tire pressure. For F_0 = 25 N, the displacement averaged from 11.6 mm at 3 bar to 9.1 mm at 8 bar, and for F_0 = 200 N, from 18.5 mm to 16.0 mm. This corresponds to a reduction in pressure center displacement of approximately 15–20% as the pressure increased. At lower pressures (3–4 bar), the $x_0(F_0)$ relationship exhibited a nonlinear character resulting from the higher compliance of the tire and the effects of hysteresis and energy losses in the rubber material (56,57). In this range, significant tire deformation and a nonuniform pressure distribution were observed, promoting a rearward shift of the contact center. Increasing the pressure reduced tire deflection and minimized the hysteresis effect, making the $x_0(F_0)$ relationship more linear and predictable (24,58). For pressures above 6 bar, the characteristics were nearly parallel, indicating stabilized contact stiffness and a more uniform pressure distribution in the contact zone (59,60). Under these conditions, the tire behaved like an elastic element with low compliance, and the $x_0(F_0, p_t)$ relationship could be accurately described by a linear model, justifying the use of a simplified approximation in further analysis.

The high coefficient of determination (R^2 = 0.957) confirmed that the model exhibited an excellent fit to the experimental data. Regression analysis demonstrated statistical significance for both the effect of normal load ($p < 0.001$) and tire pressure ($p < 0.001$). The F-test ($F(2,45) = 499.3$; $p < 0.0001$) confirmed that the model significantly explained the variability in the displacement of the pressure center. Verification of regression assumptions showed that the residuals followed a normal distribution ($p > 0.05$) and that there was no multicollinearity between independent variables (VIF < 2). These findings confirm that the model is computationally stable and reliable within the range of F_0 = 25–200 N and p_t = 3–8 bar. The linear simplification was justified, as the tire manufacturer recommends operation within the pressure range of 6–10 bar, with the upper limit of 8 bar corresponding to the capabilities of standard household compressors.

From a practical standpoint, the obtained results confirm that maintaining tire pressure in the upper range of the recommended operating interval (6–8 bar) helps reduce rolling resistance torque and enhances the stability of the reverse-locking mechanism. High tire pressure reduces radial deformation, causing the pressure center to shift closer to the wheel axis and decreasing the lever arm of the resistive force. At the same time, increasing pressure did not significantly affect the slope of the $T_b(F_0)$ characteristics, indicating that the braking torque maintained a linear and predictable relationship with the normal load within the analyzed range. From an engineering perspective, the presented findings can serve as a basis for developing new wheelchair design solutions, particularly those aimed at improving the efficiency of reverse-locking mechanisms while minimizing additional rolling resistance. They also enable optimization of roller geometry and material selection based on specific elasticity parameters to achieve the desired dynamic performance of the system. In the long term, this research can be extended to include dynamic analyses of rolling phenomena and experiments employing strain gauge and optical sensors to provide spatial mapping of pressure distribution within the contact zone.

The research objectives were achieved. Relationships between the normal load (F_0), tire pressure (p_t), and braking torque (T_b) were established, and the displacement of the pressure center (x_0) was determined as a function of the analyzed parameters. The developed model successfully described the influence of tire pressure on the load distribution within the contact zone, confirming the intended goal of the study. The linear relationship between $T_b(F_0)$ was verified, and the conditions under which the tire maintains elasticity without the risk of structural damage were identified. The research hypotheses were confirmed. Increasing tire pressure reduced the rolling resistance torque and stabilized the pressure distribution, validating the initial assumptions. The linear character of the $x_0(F_0)$ relationship was partially confirmed. At low pressures (3–4 bar), the data distribution indicated a slight nonlinearity, resulting from greater tire compliance; however, this behavior could still be accurately approximated using a linear trend function.

CONCLUSIONS

The conducted research clearly confirmed that both tire pressure and roller normal load are key factors determining the pressure distribution within the contact zone and the braking torque in the roller–tire system. As the internal tire pressure increased from 3 to 8 bar, a significant reduction in braking torque (T_b) was observed – on average by 10–15% – resulting from reduced tire deformation and a shift of the pressure center toward the wheel axis. Higher tire pressure increased contact stiffness, stabilized the distribution of normal reactions, and reduced rubber material hysteresis, making the roller–tire contact more predictable as well as repeatable. At the same time, the relationship between pressure center displacement (x_0) and normal load (F_0) exhibited a quasi-linear character throughout the tested range, which was confirmed by a high coefficient of determination (R^2 = 0.957). As the normal load increased from 25 to 200 N, the value of x_0 increased by approximately 60%, while its absolute value decreased with increasing tire pressure by about 15–20%. This indicates that higher pressure not only reduces rolling resistance but also stabilizes the operation of the reverse-locking mechanism, directly improving user comfort and safety. Maintaining tire pressure at the upper limit of the operational range (6–8 bar) should be considered optimal for minimizing rolling resistance torque, ensuring contact stability, and extending the service life of the components in the reverse-locking mechanism. The obtained results provide a foundation for further work on modeling and optimizing the

design of rollers as well as module geometry to enhance the efficiency and ergonomics of manual wheelchair propulsion systems.

Acknowledgments

This research was funded by PFRON (Poland State Fund for the Rehabilitation of Disabled Persons), grant number "BEA/000068/BF/D" and "Reverse Locking Module for Wheelchairs – Functional Prototype, Operational Testing, Popularization".

REFERENCES

1. Pavlidou E, Kloosterman MGM, Buurke JH, Rietman JS, Janssen TWJ. Rolling resistance and propulsion efficiency of manual and power-assisted wheelchairs. Med Eng Phys. 2015;37(11):1105–10.
2. Ott J, Wilson-Jene H, Koontz A, Pearlman J. Evaluation of rolling resistance in manual wheelchair wheels and casters using drum-based testing. Disabil Rehabil Assist Technol. 2022;17(6):719–30.
3. Ott J, Marcus MM, Henderson T, Wilson-Jene H, Lee L, Pearlman J. Development and calibration of drum-based rolling resistance testing machine for manual wheelchair components. Technol Disabil. 2021;33(2):123–36.
4. Kwarciak AM, Yarossi M, Ramanujam A, Dyson-Hudson TA, Sisto SA. Evaluation of wheelchair tire rolling resistance using dynamometer-based coast-down tests. J Rehabil Res Dev. 2009;46(7):931–8.
5. Pomarat Z, Marsan T, Faupin A, Landon Y, Watier B. Wheelchair caster power losses due to rolling resistance on sports surfaces. Disabil Rehabil Assist Technol. 2025;20(4):1176–82.
6. Sprigle S, Huang M, Misch J. Measurement of rolling resistance and scrub torque of manual wheelchair drive wheels and casters. Assist Technol. 2022;34(1):91–103.
7. Hashizume T, Kitagawa H, Lee H, Ueda H, Yoneda I, Booka M. Biomechanics and Physiology for Propelling Wheelchair Uphill Slope. W: Stud Health Technol Informatics. IOS Press; 2015;447–54.
8. Assila N, Rushton PW, Duprey S, Begon M. Trunk and glenohumeral joint adaptations to manual wheelchair propulsion over a cross-slope: An exploratory study. Clin Biomech. 2024;111.
9. Wieczorek B, Kukla M, Warguła Ł, Giedrowicz M, Rybarczyk D. Evaluation of anti-rollback systems in manual wheelchairs: muscular activity and upper limb kinematics during propulsion. Sci Rep. 2022;12(1).
10. Hashizume T, Kitagawa H, Ueda H, Yoneda I, Booka M. Efficiency and Rolling Resistance in Manual Wheelchair Propulsion. W: Stud Health Technol Informatics. IOS Press; 2017;778–81.
11. Hoffman MD, Millet GY, Hoch AZ, Candau RB. Assessment of wheelchair drag resistance using a coasting deceleration technique. Am J Phys Med Rehabil. 2003;82(11):880–9.
12. Sauret C, Vaslin P, Lavaste F, de Saint Remy N, Cid M. Effects of user's actions on rolling resistance and wheelchair stability during handrim wheelchair propulsion in the field. Med Eng Phys. 2013;35(3):289–97.
13. Cabelguen JC, Lavaste F. Rolling resistance analysis during wheelchair movement. W: Assistive Technol Res Ser. 2010;25–7.
14. Warguła Ł, Kukla M, Wieczorek B. The impact of wheelchairs driving support systems on the rolling resistance coefficient. W: IOP Conf Ser Mater Sci Eng. Institute of Physics Publishing; 2020.
15. Pascal JP, Zaazaa KE. A study of the effect of m and n coefficients of the hertzian contact theory on railroad vehicle dynamics. W: Proc ASME Int Des Eng Tech Conf Comp Info Eng Conf, DETC. American Society of Mechanical Engineers (ASME); 2008;1893–901.
16. Teodorescu M, Votsios V, Rahnejat H. Fundamentals of impact dynamics of semi-infinite and layered solids. W: Rahnejat H, redaktor. Tribology and Dynamics of Engine and Powertrain: Fundamentals, Applications and Future Trends. Elsevier Ltd.; 2010;105–31.
17. Salaani MK. Analytical tire forces and moments with physical parameters. Tire Sci Technol. 2008;36(1):3–42.
18. Wang H, Al-Qadi IL, Stanciulescu I. Effect of surface friction on tire-pavement contact stresses during vehicle maneuvering. J Eng Mech. 2014;140(4).
19. Derbew M, Rao DN, Zeleke E. Modeling of braking thermal effect for wheel-rail contact parameters. Proc Inst Mech Eng Part F J Rail Rapid Transit. 2021;235(8):957–68.
20. LeMay J, Adair TW, Fisher A, James J, Boltman B. Air pressure and cargo weight affect the width of tire impressions. J Forensic Identif. 2008;58(6):660–5.
21. Fabela-Gallegos MJ, Hernandez-Jimenez R, Reyes-Vidales A. Effect of load and inflation pressure on contact force and pressure distribution for two types of light duty truck tires. W: SAE Techni Paper. SAE International; 2007.
22. Huang H, Yu X, Liu J, Yao Z. Asymmetry investigation on radial tire contact pressure distribution. Xitong Fangzhen Xuebao J Syst Simul. 2018;30(8):2991–8.
23. Lu D, Wang C, Pang Z, Liu Q, Zhang Y, Lin Z. Study on the influence of tire pressure to tire mechanical properties. W: IET Conf Publ. Institution of Engineering and Technology; 2016.

24. Zhang J, Zhu FS, Wu ZF. Analysis of tire's dynamic contact pressure during braking by 3-D FEM. Dongbei Daxue XuebaoJournal Northeast Univ. 2007;28(11):1652–5.
25. Tomaraee P, Mardani A, Mohebbi A, Taghavifar H. Relationships among the contact patch length and width, the tire deflection and the rolling resistance of a free-running wheel in a soil bin facility. Span J Agric Res. 2015;13(2):1–7.
26. Steyn WJ vdM., Ilse M. Evaluation of tire/surfacing/base contact stresses and texture depth. Int J Transp Sci Technol. 2015;4(1):107–18.
27. Andersson PBU, Kropp W. Time domain contact model for tyre/road interaction including nonlinear contact stiffness due to small-scale roughness. J Sound Vib. 2008;318(1–2):296–312.
28. Mousavi H, Sandu C. Experimental study of tread rubber compound effects on tire performance on ice. SAE Int J Commer Veh. 2020;13(2):99–101.
29. Warguła Ł, Lijewski P, Kukla M. Influence of non-commercial fuel supply systems on small engine SI exhaust emissions in relation to European approval regulations. Environ Sci Pollut Res. 1 sierpień 2022;29(37):55928–43.
30. Warguła Ł, Gierz Ł, Zharkevich O, Wieczorek B, Wojciechowski Ł, Perz K, i in. The influence of kinematic viscosity of oils on the energy consumption of a gear pump used for pumping oil in machines and vehicles. PLOS ONE. 2 wrzesień 2025;20(9):e0331371.
31. Alijanpour E, Russell DM. Gait phase normalization resolves the problem of different phases being compared in gait cycle normalization. J Biomech. 2024;173.
32. Sun T, Zhan H, Chen Z, Guo Q, Yan Y. Evaluating the influence of UEXO-II on human performance: A torque and muscle level analysis. Robot Auton Syst. 1 wrzesień 2025;191:105012.
33. Besselink IJM, Schmeitz AJC, Pacejka HB. An improved Magic Formula/Swift tyre model that can handle inflation pressure changes. Veh Syst Dyn. 1 grudzień 2010;48(sup1):337–52.
34. Helwig NE, Shorter KA, Ma P, Hsiao-Wecksler ET. Smoothing spline analysis of variance models: A new tool for the analysis of cyclic biomechanical data. J Biomech. 2016;49(14):3216–22.
35. Motlani S, Gurav N, Sondkar S. Vibration signal analysis of rotating machines using VoId-Kalman filter phase analysis technique. W: IEEE Int Conf Recent Trends Electron, Inf Commun Technol, RTEICT - Proc. Institute of Electrical and Electronics Engineers Inc.; 2018;1300–4.
36. Wang J, Ying H, Fu H tao, Song L fu, Ni J feng, Gao Z yang. Field experiment and numerical simulation of the dynamic responses of rigid pipes in soft soil foundations under traffic loading. Structures. 1 maj 2025;75:108739.
37. Stache JM, Robinson WJ. Estimation of Tire Contact Area Using a Radial Spring Tire Model Coupled with a Deformable Surface. W: Airfield Highw Pavements: Des, Constr, Cond Eval, Manag Pavements - Sel Pap Int Airfield Highw Pavements Conf. American Society of Civil Engineers (ASCE); 2023. s. 385–95.
38. Tian Y, Lee J, Nantung T, Haddock JE. Development of a mid-depth profile monitoring system for accelerated pavement testing. Constr Build Mater. 1 czerwiec 2017;140:1–9.
39. Ravi G, De Waele W, Nikolic K, Petrov R, Hertelé S. Numerical modelling of rolling contact fatigue damage initiation from non-metallic inclusions in bearing steel. Tribol Int. 1 luty 2023;180:108290.
40. Heinrich G, Klüppel M. Rubber friction, tread deformation and tire traction. Wear. 20 wrzesień 2008;265(7):1052–60.
41. Gabel G, Króger M. Reasons, models and experiments for unsteady friction of vehicle tires. VDI Berichte. 2007;(2014):245–59.
42. Winroth J, Andersson PBU, Kropp W. Importance of tread inertia and damping on the tyre/road contact stiffness. J Sound Vib. 13 październik 2014;333(21):5378–85.
43. Wieczorek B, Warguła Ł, Giedrowicz M. Tire deformation-based regulation of braking torque in manual wheelchairs equipped with reverse locking modules. PLOS ONE. 17 czerwiec 2025;20(6):e0325504.
44. Matsubara M, Tajiri D, Horiuchi M, Kawamura S. Evaluation of spring properties of tire sidewall under changes in inflation pressure. SAE Int J Passeng Cars - Mech Syst. 2015;8(3):825–33.
45. Sun P, Feng G, Zhou S, Qiu C, Fan J. Experimental Analysis of Radial Tire Stiffness and Grounding Characteristics. W: IOP Conf Ser Mater Sci Eng. IOP Publishing Ltd; 2019.
46. Köylü H, Tural E. Experimental investigation on effect of variations in tire pressure on control performance of ABS under μ-jump road conditions based on tire operating parameters. Trans Inst Meas Control. 2023;45(8):1525–38.
47. de Groot S, Vegter RJK, van der Woude LHV. Effect of wheelchair mass, tire type and tire pressure on physical strain and wheelchair propulsion technique. Med Eng Phys. 2013;35(10):1476–82.
48. Park SY, Kim SH, Park DJ. Effect of the air-pressure differences of the wheelchair tires on user's upper extremity muscle activities and acceleration changes. Int J Eng Res Technol. 2020;13(11):3266–71.
49. Leboeuf A, Binot S, Weissland T. Effect of a low tire pressure on performance in wheelchair basketball players. Sci Sports. 2017;32(6):327–33.

50. Booka M, Oku H, Yoneda I, Fujisawa S. Effect of tire pressure to driving forces at a wheelchair. W: Adv Intell Sys Comput. Springer Verlag; 2017;171–81.
51. Booka M, Yoneda I, Hashizume T, Lee H, Oku H, Fujisawa S. Effect of Tire Pressure to Physical Workload at Operating a Manual Wheelchair. W: Stud Health Technol Informatics. IOS Press; 2015;929–34.
52. Liu Q, Zheng F, Hu D, Wang D, Lyu L, Wang H, i in. Analysis of the tire-pavement contact characteristics in static and dynamic conditions based on Abaqus. Int J Pavement Eng. 2025;26(1).
53. Köylü H, Tural E. Experimental investigation on effect of variations in tire pressure on control performance of ABS under μ-jump road conditions based on tire operating parameters. Trans Inst Meas Control. 2023;45(8):1525–38.
54. Fujisawa S, Sato K, Ito S ichi, Kawata J, Morimoto J, Higuchi M, i in. Effects of tire pressure on wheelchairs when riding on uneven ground. W: Adv Intell Sys Comput. Springer; 2020. s. 920–7.
55. Booka M, Fujisawa S, Oku H, Yoneda I. Influence of tire pressure to workload for manipulating a wheelchair. W: IEEJ Trans Electron Inf Syst. Institute of Electrical Engineers of Japan; 2017;40–5.
56. Assaad M, Ebbott T, Jiang B, Rebel G. Rubber comprehensive constitutive equation and the prediction of tire temperature and rolling resistance. Tire Sci Technol. 2023;51(3):162–81.
57. Jha NK, Dobriyal R, Kumar P, Badhotiya GK. On the modelling of nonlinear viscoelastic relation for rubber-like materials. W: Mater Today Proc. Elsevier Ltd; 2021;10546–50.
58. Bhave T, Tehrani M, Ali M, Sarvestani A. Hysteresis friction and nonlinear viscoelasticity of rubber composites. Compos Commun. 2018;9:92–7.
59. Wang W, Yan S, Zhao Y. Numerical and experimental studies of a radial truck tire with tread pattern. Simulation. 2015;91(11):970–9.
60. Shu YP, Chen QH, Zheng JR. Finite element analysis for steady-state rolling of radial truck tire. Huadong Ligong Daxue Xuebao J East China Univ Sci Technol. 2008;34(6):902–7.